Spurious Late Historical-Era Warming in CESM2 Driven by Prescribed Biomass Burning Emissions

J. T. Fasullo[*1,2], Jean-Francois Lamarque[1], Cecile Hannay[1], Nan Rosenbloom[1], Simone Tilmes[1], Patricia DeRepentigny[2], Alexandra Jahn[2], and Clara Deser[1]

[1]National Center for Atmospheric Research, Boulder, CO, USA.

[2]Department of Atmospheric and Oceanic Sciences and Institute of Arctic and Alpine Research, University of Colorado, Boulder, CO, USA.

[*]Corresponding author: fasullo@ucar.edu

Key Points:

- CMIP6 prescribed biomass burning emissions contain elevated interannual variance from 1997-2014 relative to other periods
- In CESM2, the variability in emissions drives substantial warming in the Northern Hemisphere extratropics
- Changes in radiation and clouds arising from nonlinear interactions with aerosols underpin the simulated warming

Abstract

A spurious increase in the interannual variability of prescribed biomass burning (BB) emissions in the CMIP6 forcing database during the satellite era of wildfire monitoring (1997-2014) is found to lead to warming in the northern hemisphere extratropics in simulations with the Community Earth System Model version 2 (CESM2). Using targeted sensitivity experiments with the CESM2 in which prescribed BB emissions are homogenized and variability is removed, we show that the warming is specifically attributable to BB variability from 40^{o}N-70^{o}N and arises from a net thinning of the cloud field and an associated increase in absorbed solar radiation. Our results also demonstrate the potential pitfalls of introducing discontinuities in climate forcing datasets when trying to incorporate novel observations.

Plain Language Summary

A discontinuity in the variability of prescribed biomass burning emissions between the satellite era of wildfire monitoring (1997-2014) and both the preceding historical and future time periods is found to drive spurious warming in the Community Earth System Model version 2. The warming arises from a net thinning of the cloud field and an associated increase in absorbed solar radiation during periods of high variability in emissions. Evidence suggestive of similar effects in other climate models is also presented. The results highlight the challenges in evaluating models with observations, even in the modern satellite era.

1 Introduction

Quantifying the sensitivity of climate to external forcing is necessary in order to accurately project the impacts of climate change and anticipate appropriate adaptation needs. Many of the most recent climate model versions exhibit estimated equilibrium responses to

carbon dioxide doubling that are considerably higher than previous model generations (Meehl et al. 2020, Zelinka et al. 2020). These most recent model versions are the result of a sustained effort by climate research groups over the past decade to improve model physics, and specifically, their representation of clouds and feedback relevant processes (Andrews et al. 2019; Gettelman et al. 2019; Golaz et al. 2019; Lohmann et al. 2018; Wyser et al. 2019). This development process has been informed by an unprecedented data record used to guide improvements in the representation of clouds and cloud-aerosol interactions (Bender et al. 2019; Kay et al. 2016; Storelvmo et al. 2017; Tan et al. 2016) that have helped drive high sensitivities (Andrews et al. 2019; Gettelman et al. 2019; Lohmann et al. 2018; Tan et al. 2016; Wyser et al. 2019). An objective assessment of performance across model generations has concluded that many of the latest versions significantly outperform older models in reproducing observed feedback-relevant fields, with some of the highest sensitivity models agreeing most closely with observations (Fasullo, 2020). However, other recent studies aimed at evaluating simulated warming have cast doubt on the reliability of high sensitivity models (Flynn and Mauritsen 2020, McKitrick and Christy 2020, Nijsse et al. 2020, Tokarska et al. 2020).

The use of the observational record to rule out high model sensitivities is on its own somewhat surprising given that the transient climate responses of recent models are only marginally larger than of earlier generations (Flynn and Mauritsen 2020, Meehl et al. 2020). Historical-era simulations rely on estimation of climate forcing, which itself introduces substantial uncertainty (Smith et al. 2020). Apparent inter-model contrasts, both across and within model generations, can thus arise from these uncertainties and the range of model sensitivities to them.

The focus of this work is on the climate response to regime changes in the interannual variability of biomass burning (BB) emissions prescribed in the most recent Coupled Model Intercomparison Project Version 6 (CMIP6) database (van Marle et al. 2017; BB emissions include sulfur dioxide, black carbon, and organic carbons). In constructing these data, observed interannual variability was retained during the duration of the Global Fire Emissions Database (GFED; van Der Werf et al. 2017), with the deleterious effect of creating such an artificial regime change. Here, we show that the associated increase in the variability of BB emissions during the GFED era leads to a net warming in the Community Earth System Model version 2 (CESM2) via decreased mean cloud droplet number and low cloud amount. The anomalous warming abates in future projections as BB variability is again small. We also present evidence suggestive of the potential for a similar response in some CMIP6 models. In a related paper, the associated responses of Arctic sea ice and climate to this forcing are examined (DeRepentigny et al. 2021).

2 Data and Methods

2.1 The Community Earth System Model

Simulations from the CESM version 2 (CESM2, Danabasoglu et al. 2020) are taken from the 11-member historical-era submission to CMIP6 (Eyring et al. 2016) and the 3-member 21st century submission for Shared Socioeconomic Pathway (SSP) 3-7.0 (O'Neill et al. 2016). The CESM2 uses the Modal Aerosol Model version 4 (Liu et al. 2016) and cloud-aerosol interactions use the updated Morrison and Gettelman scheme (MG2; Morrison and Gettelman 2008).

To provide context for the CESM2 simulations that are the focus of this work, we also consider simulations from the 40-member Community Earth System Model version 1 (CESM1) Large

Ensemble (Kay et al. 2015). These simulations provide a robust estimate of the climate response to forcing in the presence of internal variability without large interannual variability in BB emissions. The CESM1 uses the Modal Aerosol Model version 3 (MAM3, Hurrell et al. 2013) and cloud-aerosol interactions are represented through the MG1 cloud microphysics scheme (Morrison and Gettelman 2015). Emissions of aerosols and aerosol precursors in CESM1 follow Lamarque et al. (2010). Differences between the treatment of cloud-aerosol interactions in CESM1 and CESM2 are complex and relate to both changes in the treatment of aerosols, clouds, and their microphysical interactions (Danabasoglu et al. 2020, Gettelman et al. 2019, Tilmes et al. 2019,). Important differences also exist in the prescribed forcings used in each model (e.g. Smith and Forster, 2021).

2.2 CMIP6 Forcings and Homogenized Sensitivity Forcing.

Experiments are conducted to quantify the climate response resulting solely from regime changes in CMIP6 BB emission variability associated with changing data sources in 1997 as documented in van Marle et al. (2017) for northern high latitudes (discussed in section 3.1). With this goal in mind, a revised emissions dataset is created in which interannual variability is removed only from the latitude band 40^{o}N-70^{o}N over the 1997-2014 period while the integrated amount of emissions is retained. This "homogenized" dataset, which largely removes regime changes in variability in the late 20th century, is then used to create a 20-member ensemble of simulations, referred to hereafter as the CESM2BB ensemble, using otherwise identical forcing and initial conditions as the 11-member CESM2 CMIP6 ensemble. The homogenized region is chosen to coincide with the regional definitions used in van Marle et al. (2017). This approach, identical in nature to what was used in CMIP5 (Lamarque et al. 2010), removes any sharp transition with the prescribed SSP BB emissions, which are based on the GFED emissions. We then conduct a 20-

member ensemble of sensitivity simulations initialized in 1990 but using the artificial set of emissions over the period 1997-2014, with identical initial conditions as in our original CESM2 ensemble (see section 2.1).

2.3 CMIP simulations

Historical CMIP6 simulations for which at least 4 members have been provided with downwelling surface shortwave radiation (SW_{dn}) through the Earth System Grid Federation (ESGF) have been included in our analysis. CMIP experiment output is available on the ESGF (https://www.earthsystemgrid.org). As upwelling shortwave radiation is not submitted by many centers in the CMIP3 database, and because differences between net and downwelling anomalies are small, SW_{dn} is used rather than net surface shortwave radiation in evaluation of CMIP simulations.

2.4 Observations

Observed estimates of near surface (2 m) air temperature in the historical era are from the Berkeley Earth System (Rohde and Hausfather 2020). These data are well-suited for climate model evaluation as regions and times without observations are infilled to provide continuous fields. Radiative fluxes at top-of-atmosphere and the surface are from the Clouds and the Earths Radiant Energy System (CERES) database (Kato et al. 2018, Loeb et al. 2018). Tropospheric temperatures are from the European Center for Medium Range Weather Forecasts Reanalysis Version 5 (Hersbach et al. 2020). These estimates are derived from model assimilation of a broad database of in-situ and satellite observations during the GFED era.

3 Results

3.1 Simulated Late Historical-Era Climate

The transient climate responses over recent decades in the CESM1 40-member Large Ensemble (Kay et al. 2015) and an 11-member ensemble of CESM2 (Danabasoglu et al. 2020) are examined and compared to observations in order to understand the temporal and regional structure of their contrasts (Figure 1). Notably, this type of comparison is analogous in many ways to ongoing comparisons of the CMIP5 and CMIP6 archives.

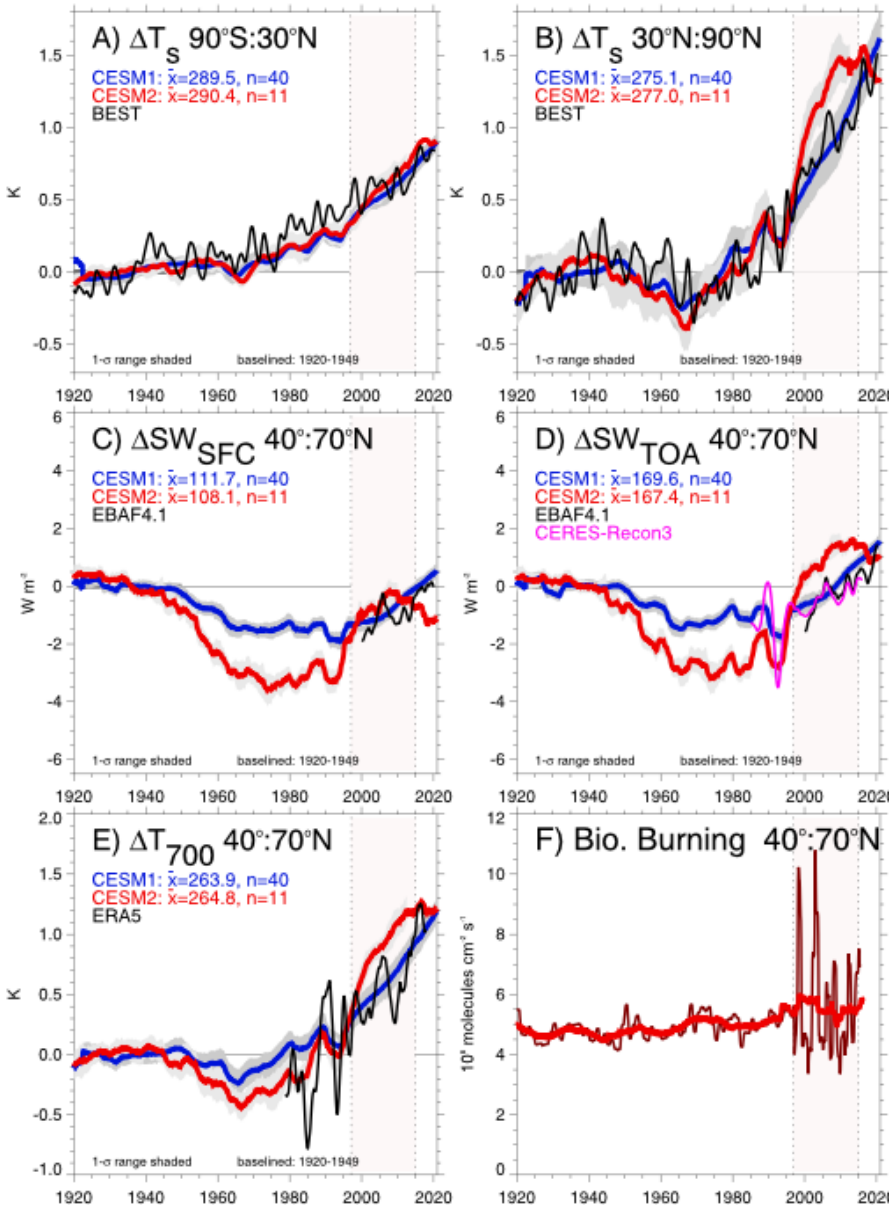

Figure 1. Historical-era evolution of large-scale climate anomalies and CMIP6 forcing including near surface air temperature averaged from 90°S-30°N (a) and 30°N-90°N (b), and mean 40°N-70°N surface net solar radiation (c), top-of-atmosphere net solar radiation (d), and 700 hPa air temperature (e). Prescribed BB emissions are also shown (f). The 1997 to 2014 era is shaded on all panels. Data include fields from the CESM1 (blue) and CESM2 (red) and observations (black/magenta, see section 2.4). Anomalies are computed relative to the 1920-49 baseline except in (f) where they are raw values. Shaded regions around a line denote the standard deviation ranges of annual mean anomalies, which for the CESM2 is also approximately equal to the 3-standard error range. Time series have been smoothed with a 5-year running mean, with the exception of BB emissions which are smoothed with 12-month (dark red) and 120-month (light red) running means.

The broad evolution of temperature in the two models before 1997 is similar, with both ensembles depicting persistent net warming, interrupted by cooling from 1950 to 1970 in the northern extratropics (Figures 1a and 1b). While observations generally fall within the ensemble spreads of both models (Figures 1a and 1b), differences in warming exist in some eras and regions, as both model versions depict somewhat less warming than observed from 1975 to 1997. Particularly notable is that from 1997 to 2010, the warming in the latitude band 30°-90°N in the CESM2 is considerably greater than either that observed or that simulated by the CESM1, as the ensemble bounds (shaded) diverge from each other starkly by 2010. Ensemble mean warming in the CESM2 is also negligible from about 2010 to 2020 before increasing again after 2020 in close agreement with warming in the CESM1 (not shown). Associated with the enhanced northern extratropical warming rate in CESM2 is an abrupt increase in the surface net solar flux (SW_{sfc}) in a narrower latitude band, from 40°N-70°N (Figure 1c), an increase that runs counter to

148 the model's historical-era decrease prior to 1997, which is considerably larger than reductions in
149 CESM1. Note the band shown for radiation anomalies (Figure 1b-d) is narrower than that for
150 surface temperature (Figure 1b) given the broad scale of the response to a relatively confined
151 band of radiation anomalies. The stronger SW_{sfc} decrease in CESM2 versus CESM1 from 1950
152 to 1990 is consistent with differences generally between CMIP6 and CMIP5, which have been
153 shown to be attributable to the combined influences of model sensitivity and contrasts in aerosol
154 and greenhouse gas forcings (Smith and Forster 2021). An abrupt increase in TOA solar flux
155 (SW_{toa}, Figure 1d) also occurs in 1997 and both are approximately 2 W m^{-2} in magnitude. The
156 enhanced warming in CESM2 is evident through much of the lower troposphere, which is
157 discussed in greater detail below, and illustrated in the evolution of 700 hPa temperature (Figure
158 1e). The period of enhanced warming also coincides with a sudden shift in the observational
159 datasets used to produce the wildfire emissions (Figure 1f), as 1997 marks the beginning of the
160 GFED observations. The GFED era (1997-2014; shaded in all panels of Figure 1) is associated
161 with a marked increase in the variability of BB emissions from 40°N-70°N, mainly in the boreal
162 Asian (BOAS) region and secondarily in the boreal North American (BONA) region (van Marle
163 et al. 2017). This creates sharp discontinuities in prescribed forcing variability, both in 1997 and
164 2014, before and after (not shown) which interannual variations are small. Contrasting changes
165 between CESM1 and CESM2 are documented in the SI while specific mechanisms that may be
166 at play in driving these changes are discussed further below.

167 **3.2 Results of Targeted Sensitivity Simulations**

168 To establish causality, and to demonstrate the importance of what might otherwise be perceived
169 as small differences in clouds and radiation between CESM1 and CESM2, the CESM2 and
170 CESM2BB ensembles are contrasted.

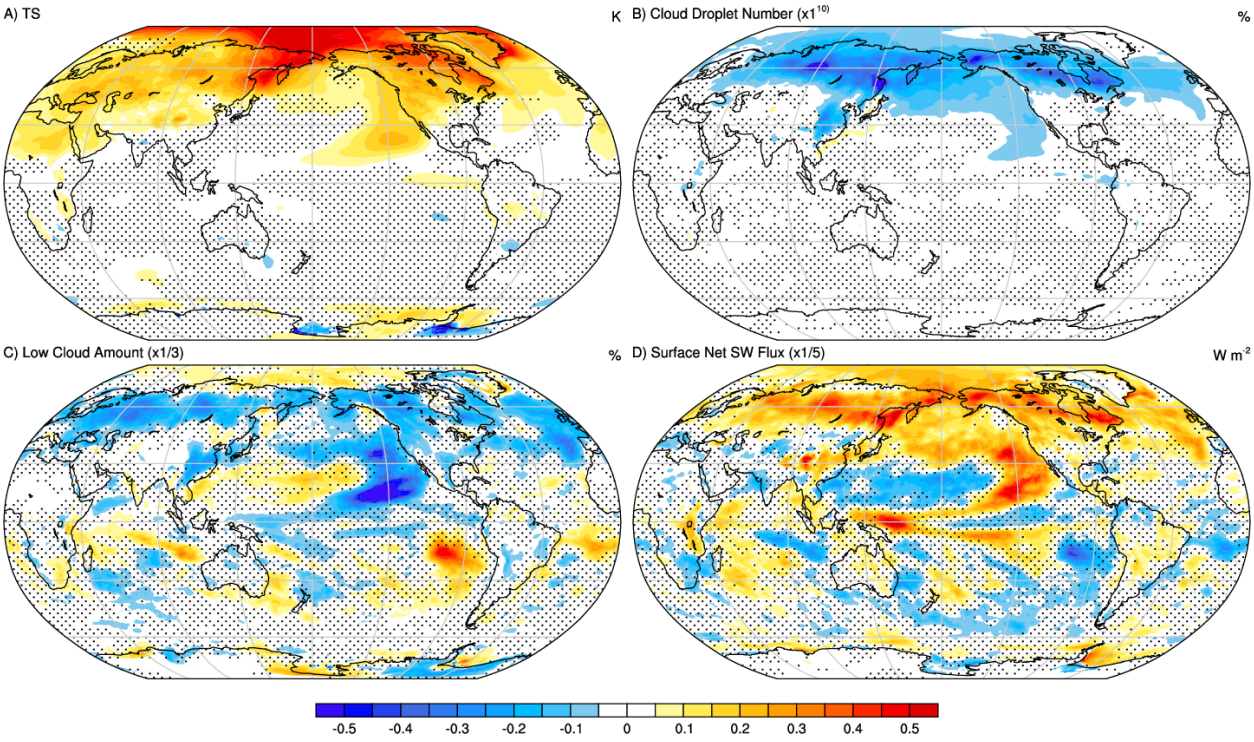

171

Figure 2. Impact of variable BB emissions on the spatial structure of late historical-era changes. Shown are CESM2 minus CESM2BB differences in 1995 to 2014 annual mean near surface air temperature (a), vertically integrated cloud droplet number (b), low cloud amount (c), and net surface shortwave flux (d). Regions where the difference in changes is less than the ensemble standard error are stippled. Note that a scaling is applied to the low cloud and surface SW flux fields as indicated in titles in panels (c/d).

172 The effect of variability during the GFED era is estimated by differencing the CESM2 and
173 CESM2BB ensemble means to resolve their geographical (Figure 2), vertical (Figure 3), and
174 temporal characteristics (Figure 4). The net effect of BB variability is to warm surface air

temperature in the Northern Hemisphere, particularly over land and north of 30°N, in excess of 1°C in some regions (Figure 2a) while having only marginal effects in regions south of 30°N. We note that while the sensitivity tests used here are based on experiments that impose smoothed emissions from 40°N-70°N, other experiments in which emissions are smoothed globally, such as the CESM2 Large Ensemble (Rodgers et al. 2021), also show marginal effects in regions south of 30°N (not shown). Associated decreases in cloud droplet number and low cloud amount are also simulated (Figures 2b and 2c), particularly in the BOAS and BONA regions, where the largest emissions occur, with strong downstream effects over the eastern subtropical Pacific Ocean evident in the low cloud field (Figure 2c) and SW_{sfc} (Figure 2d). As a result of changes in clouds, SW_{sfc} is increased across much of the Northern Hemisphere north of 30°N and over northern extratropical land regions, contributing significantly to the strong warming evident in CESM2 CMIP6 simulations.

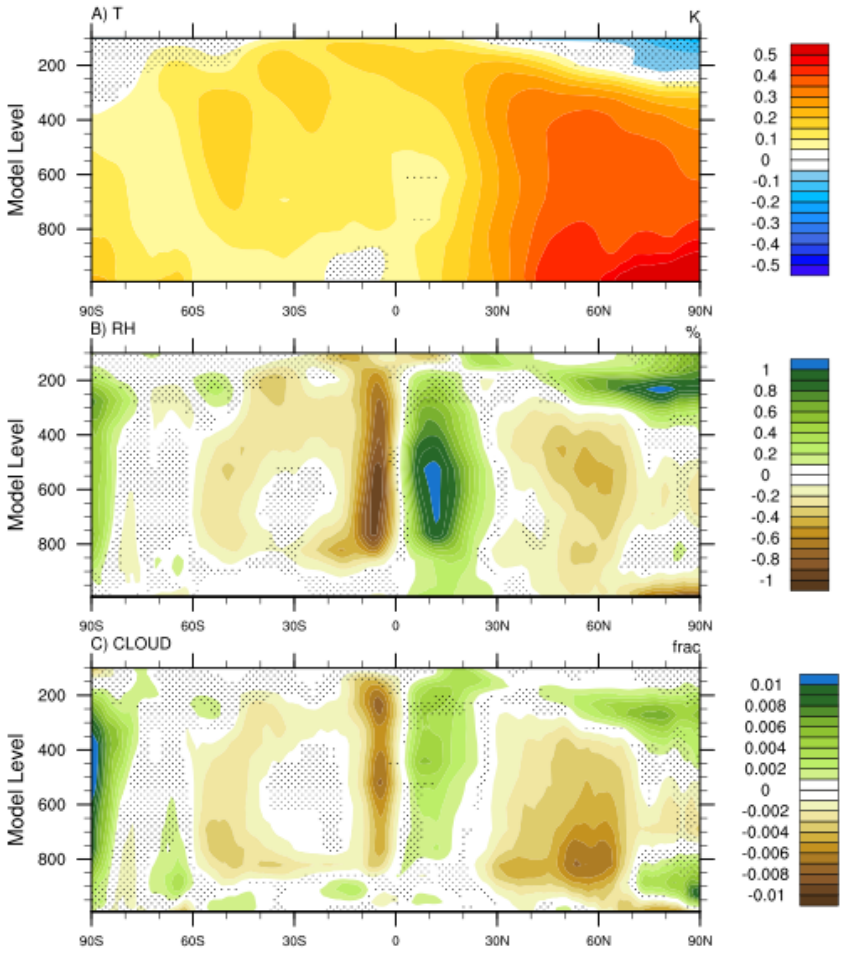

Figure 3. Impact of adjusted BB emissions on the vertical structure of late historical-era changes. Shown are CESM2 minus CESM2BB differences from 1995-2014 in temperature (a) and relative humidity (b), and cloud amount (c). Stippled regions are where differences fail to exceed the ensemble standard error.

The vertical structure of the response to BB variability is also noteworthy (Figure 3), where differences between CESM2 and CESM2BB are shown for temperature, relative humidity (RH), and cloud amount. A strong spatial coherence exists between surface (Figure 2a) and tropospheric warming (Figure 3a), with detectible warming extending from the surface, where contrasts are largest, through the depth of the troposphere and across all latitudes. South of 30ºN, warming is stronger in the free troposphere than near the surface at many latitudes. Coherent

198 with the tropospheric warming response is a decrease in RH spanning from 30°N-70°N, from the
199 surface through 500 hPa. Interestingly a remote response is also apparent, both in the tropics
200 where a southward displacement of the Intertropical Convergence Zone (ITCZ) is evident, and in
201 the Southern Hemisphere where RH decreases above the boundary layer and through much of
202 the mid- to upper-troposphere. Coincident with RH decreases are decreases in cloud amount
203 (Figure 3c), which are particularly strong below 850 hPa, that extend roughly from 20°N-70°N in
204 the Northern Hemisphere and from the equator to 60°S in the Southern Hemisphere. The strong
205 ITCZ changes noted in RH are also evident in cloud amount. The main features of these inter-
206 model differences are statistically significant and strong physical ties are known to directly link
207 the fields (e.g. RH and cloud amount), bolstering the case that they are causally linked.

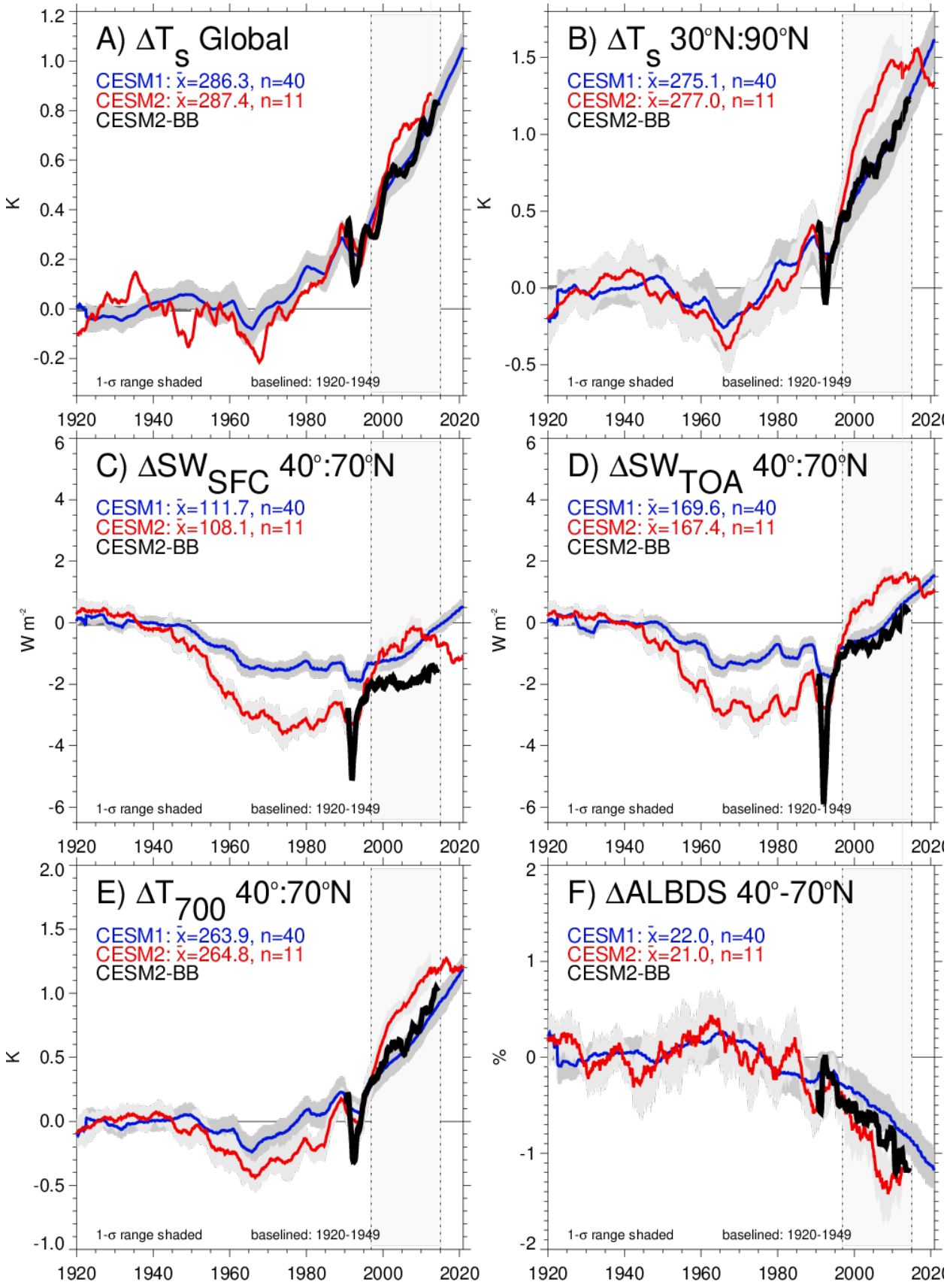
A) ΔT$_s$ Global
CESM1: x̄=286.3, n=40
CESM2: x̄=287.4, n=11
CESM2-BB
K
1-σ range shaded
baselined: 1920-1949
B) ΔT$_s$ 30°N:90°N
CESM1: x̄=275.1, n=40
CESM2: x̄=277.0, n=11
CESM2-BB
K
1-σ range shaded
baselined: 1920-1949
C) ΔSW$_{SFC}$ 40°:70°N
CESM1: x̄=111.7, n=40
CESM2: x̄=108.1, n=11
CESM2-BB
W m^{-2}
1-σ range shaded
baselined: 1920-1949
D) ΔSW$_{TOA}$ 40°:70°N
CESM1: x̄=169.6, n=40
CESM2: x̄=167.4, n=11
CESM2-BB
W m^{-2}
1-σ range shaded
baselined: 1920-1949
E) ΔT$_{700}$ 40°:70°N
CESM1: x̄=263.9, n=40
CESM2: x̄=264.8, n=11
CESM2-BB
K
1-σ range shaded
baselined: 1920-1949
F) ΔALBDS 40°-70°N
CESM1: x̄=22.0, n=40
CESM2: x̄=21.0, n=11
CESM2-BB
%
1-σ range shaded
baselined: 1920-1949

Figure 4. Similar to Figure 1 but where CESM2BB simulations (black curves) are plotted in place of observations, and panel (a) shows global near surface air temperature anomalies and panel (f) shows 40°N-70°N surface albedo anomalies. The 5-yr smoothing applied to the 25-yr CESM2BB simulations results in heightened noise near the endpoints, particularly 1990.

The temporal evolution of radiation and temperature (Figure 4) demonstrates a significant reduction of differences between CESM1 and CESM2 in depicting large-scale transient changes during the GFED era as a result of BB homogenization. Both the global and northern extratropical magnitude of warming during the era (Figures 4a and 4b) are indistinguishable between CESM1 and CESM2BB, lying well within the ensemble spread. Regional changes in ensemble mean SW_{sfc} anomalies (Figure 4c) are also very similar in the model versions, though CESM2 and CESM2BB are offset to be slightly lower than CESM1, likely due to differences in model physics and other forcing agents. At TOA, SW_{toa} anomalies in CESM2BB track closely with CESM1 (Figure 4d) and are well within the ensemble spread, while at 700 hPa, warming aligns closely with that of CESM1 (Figure 4e). Lastly, reductions in surface albedo during the GFED era (Figure 4f), which are disproportionate in CESM2, are largely consistent between CESM1 and CESM2BB, though the ensemble mean of CESM2BB decreases somewhat more than that of CESM1. Contributions to the reduction in surface albedo arise from both land and ocean regions (not shown) and raise the issue of changes in the cryosphere, their sensitivity to warming, and their role as a feedback agent that amplifies the radiative response to BB emissions. Aspects of feedbacks related to Arctic sea ice are addressed in a companion manuscript (DeRepentingy et al. 2021). Many of the disparities in GFED-era trends between CESM2 and CESM2BB are short-lived, as the ensemble averages align more closely in many

fields by the end of the historical era. (Figure 4). The alignment may result in part from the relatively small variability late in the GFED record compared to that in its early years (Figure 1f). As a consequence, the computation of trends over time periods that involve the GFED era are likely to have a spurious contribution from the response to variable BB forcings. While it remains to be explicitly quantified, the suggestion here (Figures 4a and 4b) is that these effects on temperature are likely to overshadow any differences in warming resulting from the contrasting climate sensitivities of the models (4.1^{o}C for CESM1 and 5.3^{o}C for CESM2), given the close agreement of CESM1 and CESM2BB time series.

3.3 CMIP6 Climate Simulations

The demonstrated sensitivity of CESM2 to prescribed BB emissions raises the associated question as to whether other CMIP6 climate models exhibit similar sensitivities. While it is beyond the scope of this work to perform additional targeted experiments with other models, it is possible to examine transient changes in surface downwelling solar flux (SW_{dn}) as an indicator of potential BB responses. It is also of general interest to know whether there is a systematic shift between earlier generations of CMIP simulations and the most recent generation, CMIP6. The evolution of ensemble-mean SW_{dn} anomalies (Figure S2a), relative to the 1970-1990 mean, indeed exhibits a significant positive average anomaly of 0.7 Wm^{-2} across the GFED era for CMIP6, while being near zero (~0.1 W m^{-2}) for the two prior CMIP Versions (CMIP3 and CMIP5). The differences between these ensembles lie well outside of the standard deviations of annual means and further still outside of their standard errors (<0.1 Wm^{-2}). Moreover, evidence for a dependency in the strength of the effect across models also exists (Figure S2b), with individual model ensemble mean SW_{dn} anomalies during the GFED era being as much as +1.7

254 Wm^{-2} in some models (on par with CESM2 at 1.6 W m^{-2}), between 0.5 and 1.5 Wm^{-2} in over
255 80% of models, and more than the mean CMIP3/5 anomaly of 0.1 Wm^{-2} in all but one model
256 (CanESM5; -0.1 W m^{-2}). There are therefore initial indications that similar effects of variability
257 in BB emissions may exist in other simulations in the CMIP6 models and contribute to additional
258 GFED-era warming. The prospects of strong model dependency are also raised. A key question
259 is whether the contrasting changes in SW_{dn} are driven by BB or other effects, and particularly the
260 influence of anthropogenic aerosols. Further targeted experiments, similar to that performed here
261 for CESM2, are thus motivated to clarify this issue. If these early indications are validated, a
262 significant challenge exists for efforts to evaluate CMIP6 models, or attribute observed changes
263 in the late 20^{th} and early 21^{st} centuries.

264 **4 Discussion**

265 A compelling motivation exists for winnowing the range of projected future climate through
266 comparison of simulated trends with the observational record. Such efforts are surprisingly
267 challenging however as they rely implicitly on our ability to 1) accurately diagnose external
268 climate forcings over time, 2) resolve forced changes in the presence of internal variability in
269 both observations and models, and 3) establish physical ties between the drivers of present-day
270 and future trends. While much attention has been paid to the uncertainties in anthropogenic
271 industrial aerosol emissions and their effects, it is shown here that climate forcings sometimes
272 thought of as being of secondary importance, such as BB, can be important.
273 Some aspects of the climate response in CESM2 remain to be fully understood, such as the
274 influence of BB emission variability on aerosol burdens, size droplet distributions, and cloud
275 microphysics. While BB aerosols are an absorber of solar radiation, they also interact directly
276 with cloud microphysical schemes. Are the microphysical interactions important, and if so, what

role do they play? Moreover, the fact that our homogenized dataset yields a distinct climate response, despite retaining the same monthly mean bulk emissions as the original CMIP6 emissions, suggests that the response must be intrinsically nonlinear. The origin of nonlinearities may stem in part from the effects of aerosols on clouds (Figure 30.4 of Haywood, 1996) whereby as the number of aerosols increases, the cloud droplet response asymptotes. This asymptotic behavior is suggested in our simulations: for example, despite aerosol emissions anomalies being only slightly negative in 1997 and significantly positive 1998 (Figure 1f), anomalies in cloudy-sky albedo are strongly negative in 1997 and only marginally positive in 1998 (not shown). There is also skewness in the CMIP6 emissions themselves as relative few years of high emissions are interspersed among multiple years of slightly below average emissions. A plausible hypothesis is therefore that asymptotic behavior in cloud droplet responses combined with skewness in the emissions drive the anomalous net warming in CESM2-CMIP6 simulations.

Other potential mechanisms may also contribute to driving the nonlinear responses in CESM2. For example, the response of cloud amount itself may also be nonlinear due to the discrete RH threshold used to initiate cloud formation. Feedbacks with the cryosphere are likely to amplify the climate response and may themselves impart nonlinearity as snow and ice cover fraction are fundamentally bounded fields (i.e., 0-1). The effects of cloud and warming responses detailed here on Arctic sea ice have already been documented in CESM2 (DeRepentigny et al. 2020, 2021). The expectation of linearity is itself complicated by the strong dependence of both forcings and feedbacks on season at high latitudes, as small shifts in time and space of a forcing agent can significantly modulate its net radiative effect. Ultimately, additional sensitivity experiments will be needed for a full understanding of the mechanisms involved.

The results of this work have broad relevance for interpreting previous efforts and guiding future follow-on work. Some recent studies, for example, may have conflated the climate response to BB with the climate feedbacks that drive climate sensitivity. This is evident for example in cases where spatial patterns of warming are used to attribute causality to greenhouse gases (GHG, Tokarska et al. 2020), as the BB response is spatially correlated with that response (Figure 2). Moreover, attempts to reduce the influence of uncertainty in aerosol forcing by extending analysis of trends into recent decades (Nijsse et al. 2020) remain vulnerable to the spurious effects induced by BB. Notably, the possibility exists that model physics that may render certain models more susceptible to the effects of BB emissions, such as those with more advanced representations of cloud microphysics in CMIP6 models (Andrews et al. 2019, Gettelman et al. 2019, Golaz et al. 2019, Lohmann et al. 2018, Wyser et al. 2019, Zelinka et al. 2020). This in turn may provide a statistical basis for perceived links of recent warming to higher inferred climate sensitivity. Given this, it remains a challenge to reduce the uncertainty in future projections in CMIP6 through comparison with recent observed trends.

Lastly, the findings of this work also call into question standard techniques for estimating internal variability from extended preindustrial simulations, which almost always lack variable BB emissions. Here it is shown that such emissions are an important component of the climate system, with the potential to significantly alter clouds, temperature, and radiation on timescales from seasons to (at least) decades. When forced with realistic variability in BB emissions, multiple positive feedbacks are likely to be triggered (e.g. clouds, cryosphere), thus increasing the potential range of variability. Moreover, as land model component capabilities improve, many models now include the ability to explicitly simulate BB emissions. This capability provides the opportunity to represent BB emissions as an internal climate process. Explicit

representation of the emissions has the implicit advantage of allowing for climate state dependence of emissions and their feedbacks across a range of past and future time periods. Doing so seems particularly important given known links between wildfire and climate. Paths forward for further constraining climate sensitivity are less obvious. Continued scrutiny of models with a diverse and expanding observational record, and particularly with a focus on process-relevant fields (e.g. Fasullo 2020) is likely to provide useful information regarding model fidelity. Consideration of the climate response across paleoclimate timescales (Zhu et al. 2020) and in combined statistical assessments (Sherwood et al. 2020) is also likely to provide useful information. Ultimately, coordinated advances across this broad range of climate monitoring and modeling disciplines will be essential for further reducing uncertainty in projections of the climate system's response to external forcing.

Acknowledgments, Samples, and Data

This material is based upon work supported by the National Center for Atmospheric Research, which is a major facility sponsored by the National Science Foundation (NSF) under Cooperative Agreement 1852977. The CESM project is supported primarily by the NSF. Computing and data storage resources, including the Cheyenne supercomputer (doi:10.5065/D6RX99HX), were provided by the Computational and Information Systems Laboratory (CISL) at NCAR. We thank all the scientists, software engineers, and administrators who contributed to the development of CESM2. The efforts of Dr. Fasullo in this work were partially supported by NASA Award 80NSSC17K0565 and the Regional and Global Model Analysis (RGMA) component of the Earth and Environmental System Modeling Program of the U.S. Department of Energy's Office of Biological and Environmental Research (BER) via National Science Foundation IA 1844590. The efforts of Dr. Fasullo in this work were also supported in part by NSF Award AGS-1419571. We acknowledge the World Climate Research Programme, which, through its Working Group on Coupled Modelling, coordinated and promoted CMIP6. We thank the climate modeling groups for producing and making available their model output, the Earth System Grid Federation (ESGF) for archiving the data and providing access, and the multiple funding agencies who support CMIP6 and ESGF. The authors would like to acknowledge the efforts of three anonymous reviewers in providing helpful comments on an earlier version of this manuscript.

Author contributions

JF initiated this study, contributed to the experiment design, analyzed results, prepared the figures, and first manuscript. JFL contributed to experiment design and manuscript revisions. CH

356 and NR produced the sensitivity simulations. PD, ST, CD, and AJ contributed to refining the
357 manuscript.

358 **Competing interests**

359 The authors declare no competing interests.

360 **Data and materials availability**

361 The data supporting the conclusions of this paper can be found on the Earth System Grid
362 Federation (https://www.earthsystemgrid.org/search.html?freeText=CESM2+CMIP6+historical
363 &Model=CESM2.1&Experiment=b.e21.BHIST.f09_g17.CMIP6-historical.003) where links to
364 specific simulation cases lead to the atmospheric fields used in this work, (e.g. such as TREFHT
365 for reference near surface air temperature). Simulation output for sensitivity simulations is
366 available on NCAR's Digital Asset Services Hub (DASH, dash.ucar.edu) under CESM2 40-70N
367 Biomass Emissions Homogenization Sensitivity Tests (https://doi.org/10.5065/7f7c-zw94).
368 CERES EBAF Ed4.1 data used here are available at https://ceres-tool.larc.nasa.gov/ord-
369 tool/jsp/EBAFTOA41Selection.jsp under the "TOA Fluxes" checkbox.

370

References

Andrews, T. Andrews, M. B. Bodas-Salcedo, A. Jones, G. S. Kuhlbrodt, T. Manners, J.... Senior, C. A., 2019: Forcings, feedbacks, and climate sensitivity in HadGEM3-GC3.1 and UKESM1, Journal of Advances in Modeling Earth Systems, 11, 4377-4394, doi: 10.1029/2019MS001866.

Bender, F. M. Frey, L. McCoy, D. T. Grosvenor, D. P. Mohrmann, J. K., 2019: Assessment of aerosol–cloud–radiation correlations in satellite observations, climate models and reanalysis. Climate Dynamics, 52, 4371-4392, 10.1007/s00382-018-4384-z.

Danabasoglu, G. Lamarque, J. F. Bacmeister, J. Bailey, D. A. DuVivier, A. K. Edwards, J.... Hannay, C. 2020: The Community Earth System Model version 2 (CESM2). Journal of Advances in Modeling Earth Systems, 12, e2019MS001916, doi: 10.1029/2019MS001916.

DeRepentigny, P. Jahn, A. Holland, M. M. Smith, A., 2020: Arctic Sea Ice in Two Configurations of the Community Earth System Model Version 2 (CESM2) During the 20th and 21st Centuries. J. Geophysical Research: Oceans, e2020JC016133, doi: 10.1029/2020JC016133.

DeRepentigny, P. Jahn, A. Holland, J. E. Kay, J. T. Fasullo, J.F. Lamarque, S. Tilmes, C. Hannay, M.J. Mills, D. A. Bailey, S. Tilmes, Barrett, A., 2021: Enhanced early 21st century Arctic sea ice loss due to CMIP6 biomass burning emissions, Nature Climate Change (2021), in revision.

Eyring, V. Bony, S. Meehl, G. A. Senior, C. A. Stevens, B. Stouffer, R. J. Taylor, K. E., 2016: Overview of the Coupled Model Intercomparison Project Phase 6 (CMIP6) experimental

393 design and organization. Geoscientific Model Development, 9, 1937-1958, doi:
394 10.5194/gmd-9-1937-2016.

395 Fasullo, J. T., 2020: Evaluating simulated climate patterns from the CMIP archives using
396 satellite and reanalysis datasets using the Climate Model Assessment Tool
397 (CMATv1). *Geoscientific Model Development*, *13*(8), 3627-3642, 10.5194/gmd-13-3627-
398 2020.

399 Flynn, C. M. Mauritsen, T., 2020: On the climate sensitivity and historical warming evolution in
400 recent coupled model ensembles, Atmos. Chem. Phys., 20, 7829–7842, doi: 10.5194/acp-
401 20-7829-2020.

402 Gettelman, A., Morrison, H., 2015: Advanced two-moment bulk microphysics for global models.
403 Part I: Off-line tests and comparison with other schemes. Journal of Climate, 28, 1268-
404 1287, doi: 10.1175/JCLI-D-14-00102.1.

405 Gettelman, A. Hannay, C. Bacmeister, J.T. Neale, R. B. Pendergrass, A. G. Danabasoglu, G.... &
406 Mills, M. J., 2020: High climate sensitivity in the Community Earth System Model
407 version 2 (CESM2). Geo. Res. Lett., 46, 8329-8337, doi: 10.1029/2019GL083978.

408 Golaz, J. C. Caldwell, P. M. Van Roekel, L. P. Petersen, M. R. Tang, Q. Wolfe, J. D., 2019: The
409 DOE E3SM coupled model version 1: Overview and evaluation at standard resolution. J.
410 Adv. Modeling Earth Systems, 11, 2089–2129, doi: 10.1029/2018MS001603.

411 Haywood, J. 2021: Atmospheric aerosols and their role in climate change. In *Climate*
412 *change* (pp. 645-659). Elsevier, doi: 10.1016/B978-0-12-821575-3.00030-X.

413 Hersbach, H, Bell, B. Berrisford, P. Hirahara, S. Horányi, A. Muñoz-Sabater, J.... Simmons,A.
414 The ERA5 global reanalysis. Quar. J. Royal Met. Soc., 146, 1999-2049, doi:
415 10.1002/qj.3803.

416 Hurrell, J. W. Holland, M. M. Gent, P. R. Ghan, S. Kay, J. E. Kushner, P. J. ... Lipscomb, W. H.,
417 2013: The community earth system model: a framework for collaborative research. Bull.
418 Amer. Met. Soc, 94, 1339-1360, doi: 10.1175/BAMS-D-12-00121.1.

419 Kato, S. Rose, F. G. Rutan, D. A. Thorsen, T. J. Loeb, N. G. Doelling, D. R.... Ham, S. H.
420 Surface irradiances of edition 4.0 clouds and the earth's radiant energy system (CERES)
421 energy balanced and filled (EBAF) data product. J. Climate, 31, 4501-4527, doi:
422 10.1175/JCLI-D-17-0523.1.

423 Kay, J. E. Deser, C. Phillips, A. Mai, A. Hannay, C. Strand, G.... Holland, M., 2015: The
424 Community Earth System Model (CESM) large ensemble project: A community resource
425 for studying climate change in the presence of internal climate variability. Bull. Amer.
426 Met. Soc, 96, 1333-1349, doi: 10.1175/BAMS-D-13-00255.1.

427 Kay, J. E. L'Ecuyer, T. Chepfer, H. Loeb, N. Morrison, N., A. Cesana, G., 2016: Recent
428 advances in Arctic cloud and climate research. Current Climate Change Reports, 2, 159-
429 169, doi: 10.1007/s40641-016-0051-9.

430 Lamarque, J. F. Bond, T. C. Eyring, V. Granier, C. Heil, A. Klimont, … van Vuuren, D. P.,
431 2010: Historical (1850–2000) gridded anthropogenic and biomass burning emissions of
432 reactive gases and aerosols: methodology and application, Atmos. Chem. Phys., 10,
433 7017–7039, doi: 10.5194/acp-10-7017-2010.

434 Liu, X. Ma, P. L. Wang, H. Tilmes, S. Singh, B. Easter, R. C. Ghan, S. J. Rasch, P. J., 2016:
435 Description and evaluation of a new four-mode version of the Modal Aerosol Module
436 (MAM4) within version 5.3 of the Community Atmosphere Model, Geosci. Model Dev.,
437 9, 505–522, doi: 10.5194/gmd-9-505-2016.

438 Loeb, N. G. Doelling, D. R. Wang, H. Su, W. Nguyen, C Corbett, J. G.... Kato, S., 2018: Clouds
439 and the earth's radiant energy system (CERES) energy balanced and filled (EBAF) top-
440 of-atmosphere (TOA) edition-4.0 data product. J. Climate, 31, 895-918, doi:
441 10.1175/JCLI-D-17-0208.1.

442 Lohmann, U. Neubauer, D., 2018: The importance of mixed-phase and ice clouds for climate
443 sensitivity in the global aerosol-climate model ECHAM6-HAM2. Atmospheric
444 Chemistry and Physics, 18, 8807-8828, doi: 10.5194/acp-18-8807-2018.

445 McKitrick, R. Christy, J., 2020: Pervasive Warming Bias in CMIP6 Tropospheric Layers. Earth
446 and Space Science, e2020EA001281, doi: 10.1029/2020EA001281.

447 Meehl, G.A. Senior, C. A. Eyring, V. Flato, G. Lamarque, J. F. Stouffer, R. J. ... Schlund, M.,
448 2020: Context for interpreting equilibrium climate sensitivity and transient climate
449 response from the CMIP6 Earth system models. Science Advances, 6, eaba1981, doi:
450 10.1126/sciadv.aba1981.

451 Morrison, H. Gettelman, A., 2008: A new two-moment bulk stratiform cloud microphysics
452 scheme in the Community Atmosphere Model, version 3 (CAM3). Part I: Description and
453 numerical tests. J. Climate, 21, 3642-3659, doi: 10.1175/2008JCLI2105.1.

454 Nijsse, F. J. Cox, P. M., 2020: Williamson, M. S. An emergent constraint on Transient Climate
455 Response from simulated historical warming in CMIP6 models. Earth System Dynamics
456 Discussions, 2020, 1-14, doi: 10.5194/esd-2019-86.

457 O'Neill, B. C., Tebaldi, C., Vuuren, D. P. V., Eyring, V., Friedlingstein, P., Hurtt, G., ... &
458 Sanderson, B. M. (2016). The scenario model intercomparison project (ScenarioMIP) for
459 CMIP6. Geoscientific Model Development, 9(9), 3461-3482, doi: 10.5194/gmd-9-3461-
460 2016.

461 Rodgers, K. B., Lee, S.-S., Rosenbloom, N., Timmermann, A., Danabasoglu, G., Deser, C.,
462 Edwards, J., Kim, J.-E., Simpson, I., Stein, K., Stuecker, M. F., Yamaguchi, R., Bodai,
463 T., Chung, E.-S., Huang, L., Kim, W., Lamarque, J.-F., Lombardozzi, D., Wieder, W. R.,
464 and Yeager, S. G.: Ubiquity of human-induced changes in climate variability, Earth Syst.
465 Dynam. Discuss. [preprint], https://doi.org/10.5194/esd-2021-50, in review, 2021

466 Rohde, R. A. Hausfather, Z., 2020: The Berkeley Earth Land/Ocean Temperature Record, Earth
467 Syst. Sci. Data Discuss., 1-16, doi: 10.5194/essd-12-3469-2020.

468 Sherwood, S. Webb, M. J. Annan, J. D. Armour, K. C. Forster, P. M. Hargreaves, J. C. ...
469 Watanabe M., 2020: An assessment of Earth's climate sensitivity using multiple lines of
470 evidence. Reviews of Geophysics, e2019RG000678, doi: 10.1029/2019RG000678.

471 Smith, C. J. Kramer, R. J. Myhre, G. Alterskjær, K. Collins, W. Sima, A. … Yukimoto, S.
472 Effective radiative forcing and adjustments in CMIP6 models. Atmospheric Chemistry
473 and Physics, 20, 9591-9618, doi: 10.5194/acp-20-9591-2020.

474 Smith, C. J., Forster, P. M. (2021). Suppressed Late-20th Century Warming in CMIP6 Models
475 Explained by Forcing and Feedbacks. Geophysical Research Letters, 48(19), doi:
476 10.1029/2021GL094948.

477 Storelvmo, T. 2017: Aerosol effects on climate via mixed-phase and ice clouds. Annual Review
478 of Earth and Planetary Sciences, 45, 199-222, doi: 10.1146/annurev-earth-060115-
479 012240.

480 Tan, I. Storelvmo, T. Zelinka, M. D., 2016: Observational constraints on mixed-phase clouds
481 imply higher climate sensitivity. Science, 352, 224-227, doi: 10.1126/science.aad5300.

482 Tilmes, S., Hodzic, A., Emmons, L. K., Mills, M. J., Gettelman, A., Kinnison, D. E., et al.
483 (2019). Climate forcing and trends of organic aerosols in the Community Earth System
484 Model (CESM2). Journal of Advances in Modeling Earth Systems, 11, 4323–4351, doi:
485 10.1029/2019MS001827.

486 Tokarska, K. B. Stolpe, M. B. Sippel, S. Fischer, E. M. Smith, C. J. Lehner, F. Knutti, R., 2020:
487 Past warming trend constrains future warming in CMIP6 models. Science Advances,
488 6(12), eaaz9549, doi: 10.1126/sciadv.aaz9549.

489 van Marle, M. J. E. Kloster, S. Magi, B. I. Marlon, J. R. Daniau, A. L. Field, R. D.... Knorr, W.,
490 2017: Historic global biomass burning emissions for CMIP6 (BB4CMIP) based on
491 merging satellite observations with proxies and fire models (1750–2015), Geosci. Model
492 Dev., 10, 3329–3357, doi: 10.5194/gmd-10-3329-2017.

493 van der Werf, G. R. Randerson, J. T. Giglio, L. van Leeuwen, T. T. Chen, Y. Rogers, B. M. Mu,
494 M. van Marle, M. J. E. Morton, D. C. Collatz, G. J. Yokelson, R. J. Kasibhatla, P. S.,

2017: Global fire emissions estimates during 1997–2015, Earth Syst. Sci. Data Discuss., 9, 697-720, doi: 10.5194/essd-9-697-2017.

Wyser, K. Noije, T. V. Yang, S. Hardenberg, J. V. O'Donnell, D. Döscher, R., 2019: On the increased climate sensitivity in the EC-Earth model from CMIP5 to CMIP6. Geoscientific Model Development Discussions, 13, 3465-3474, doi: 10.5194/gmd-13-3465-2020.

Zelinka, M. D. Myers, T. A. McCoy, D. T. Po-Chedley, S. Caldwell, P. M. Ceppi, P. ... Taylor, K. E., 2020: Causes of higher climate sensitivity in CMIP6 models. Geo. Res. Lett., 47, e2019GL085782, doi: 10.1029/2019GL085782.

Zhu, J. Poulsen, C. J. Otto-Bliesner, B. L., 2020: High climate sensitivity in CMIP6 model not supported by paleoclimate. Nature Climate Change, 10, 378-379, doi: 10.1038/s41558-020-0764-6.